Magnetocaloric properties and critical behavior of high relative cooling power FeNiB nanoparticles

Chaudhary, V.; Maheswar Repaka, D. V.; Chaturvedi, A.; Sridhar, I.; Ramanujan, R. V.

2014

Chaudhary, V., Maheswar Repaka, D. V., Chaturvedi, A., Sridhar, I., & Ramanujan, R. V. (2014). Magnetocaloric properties and critical behavior of high relative cooling power FeNiB nanoparticles. Journal of applied physics, 116(16), 163918-.

https://hdl.handle.net/10356/102834

https://doi.org/10.1063/1.4900736

AIP | Journal of Applied Physics

Magnetocaloric properties and critical behavior of high relative cooling power FeNiB nanoparticles

V. Chaudhary, D. V. Maheswar Repaka, A. Chaturvedi, I. Sridhar, and R. V. Ramanujan

Citation: Journal of Applied Physics **116**, 163918 (2014); doi: 10.1063/1.4900736
View online: http://dx.doi.org/10.1063/1.4900736
View Table of Contents: http://scitation.aip.org/content/aip/journal/jap/116/16?ver=pdfcov
Published by the AIP Publishing

Magnetocaloric properties and critical behavior of high relative cooling power FeNiB nanoparticles

V. Chaudhary,[1,2,3] D. V. Maheswar Repaka,[3] A. Chaturvedi,[3] I. Sridhar,[4] and R. V. Ramanujan[3,a)]

[1]*Interdisciplinary Graduate School, Nanyang Technological University, Singapore 639798, Singapore*
[2]*Energy Research Institute @NTU (ERI@N), Nanyang Technological University, Singapore 637553, Singapore*
[3]*School of Materials Science and Engineering, Nanyang Technological University, Singapore 639798, Singapore*
[4]*School of Mechanical and Aerospace Engineering, Nanyang Technological University, Singapore 639798, Singapore*

(Received 1 September 2014; accepted 19 October 2014; published online 31 October 2014)

Low cost magnetocaloric nanomaterials have attracted considerable attention for energy efficient applications. We report a very high relative cooling power (RCP) in a study of the magnetocaloric effect in quenched FeNiB nanoparticles. RCP increases from 89.8 to 640 J kg^{-1} for a field change of 1 and 5 T, respectively, these values are the largest for rare earth free iron based magnetocaloric nanomaterials. To investigate the magnetocaloric behavior around the Curie temperature (T_C), the critical behavior of these quenched nanoparticles was studied. Detailed analysis of the magnetic phase transition using the modified Arrott plot, Kouvel-Fisher method, and critical isotherm plots yields critical exponents of $\beta = 0.364$, $\gamma = 1.319$, $\delta = 4.623$, and $\alpha = -0.055$, which are close to the theoretical exponents obtained from the 3D-Heisenberg model. Our results indicate that these FeNiB nanoparticles are potential candidates for magnetocaloric fluid based heat pumps and low grade waste heat recovery. © *2014 AIP Publishing LLC*. [http://dx.doi.org/10.1063/1.4900736]

I. INTRODUCTION

Environmental degradation and energy efficiency are of high interest due to global warming and finite energy resources.[1] Low grade waste heat recovery and heat pumps are of special interest because of their tremendous potential to improve energy efficiency.[2,3] Low grade waste heat is expelled to the atmosphere during production and consumption of energy, this waste heat can be recycled using the magnetocaloric effect (MCE). A heat pump is a device which can transfer heat from a cool region to a hot region.[4] MCE based heat pumps are more cost effective and energy efficient than conventional heat pumps.[5] The MCE is the change in temperature, corresponding to the magnetic entropy change (ΔS_M), of a material due to the adiabatic application (or removal) of an external magnetic field.[6,7] Generally, MCE is large close to the Curie temperature (T_C), where the magnetic spins undergo an order ↔ disorder phase transition.[8] The relative cooling power (RCP) is an important performance metric to rank magnetocaloric materials, quantifies the magnitude of heat extracted in a thermodynamic cycle.[9] High RCP, reasonable ΔS_M, as well as low thermal and magnetic hysteresis are required for MCE based heat pumps.

Gd based materials exhibit very high ΔS_M,[7,10,11] however, materials containing rare earths such as Gd are very expensive, of limited availability, involve radioactive mining, etc., which precludes large scale commercialization. On the other hand, transition metal (TM) based alloys are highly attractive to replace such rare earth based materials. TM based alloys are low cost, readily available, earth abundant, and environmentally friendly.[12] Hence, there is considerable interest in developing rare earth free magnetocaloric materials. Magnetic nanoparticles (MNPs) can exhibit superior magnetocaloric properties compared to the bulk but there are very few reports of the MCE of nanoparticles.[13,14] The RCP of nanoparticles can be increased through a broad magnetic phase transition, which will be useful for low grade waste heat recovery and heat pumps.[15] Ucar *et al.*, reviewed the RCP (in Joule/$) of various magnetocaloric materials and found that FeNi based materials are very useful for such applications.[13] For self pumping cooling systems, MNPs are suitable if the T_C lies between room temperature and the device operating temperature.[16]

Besides the urgent need for low cost MCE materials, analysis of the critical behavior of such materials is of high interest since it is directly related to the MCE.[17] The critical exponents α, β, γ, and δ correspond to specific heat, spontaneous magnetization, magnetic susceptibility, and critical isotherm, respectively. These exponents are directly related to the MCE of the materials. For example, with the help of the Arrott-Noakes equation of state, the magnetic entropy change at $T = T_C$ can be expressed by the following relations:[18]

$$\Delta S_M = \frac{-a\beta\gamma}{b^{\frac{\beta+\gamma}{\beta+\gamma}}(2\beta+\gamma-1)} H^{\frac{\beta-1}{\beta+\gamma}+1} = AH^n, \qquad (1)$$

where $n = 1 + [(\beta - 1)/(\beta + \gamma)]$, a and b are constants and A is a function of the critical exponents. The field dependence of RCP can be expressed as power law of $RCP \propto H^N$, where $N = 1 + 1/\delta$. Hence, the determination of critical

a)Electronic mail: ramanujan@ntu.edu.sg

exponents (α, β, γ and δ) is useful to evaluate the MCE performance of the materials even at high field, which may not be available in many laboratories as well as to compare the MCE results obtained by various investigators using different maximum fields. In addition, the critical behavior study is a powerful approach to understand the mechanism of the magnetic phase transition and the nature of ordering around T_C.

We report the synthesis and structure of Fe–Ni–B nanoparticles possessing a metastable face centered cubic (fcc) crystalline structure. Boron was added to reduce the T_C to ~100 °C, suitable for low grade waste heat recovery.[3] Previous work on $(Fe_{70}Ni_{30})_{89}Zr_7B_4$ nanoparticles showed attractive magnetocaloric properties.[19] However, zirconium is not preferred for waste heat recovery applications due to their pyrophoric nature. These particles have to be suspended such as water and pyrophoric materials will not be useful. Here, Zr was replaced by B and the composition of $(Fe_{70}Ni_{30})_{89}B_{11}$was selected, which is found in this work to yield superior MCE ($\Delta S_M = -2.1$ J kg^{-1} K^{-1}, RCP = 640 J kg^{-1} at $\Delta H = 5$ T) properties compared to $(Fe_{70}Ni_{30})_{89}Zr_7B_4$. The MCE is much more dramatic near T_C. Hence, the critical exponents of the magnetic phase transition near T_C were obtained using Landau's mean field model, 3D-Ising, 3D-Heisenberg, and tricritical mean field models.[20] The obtained critical exponents ($\beta = 0.364$, $\gamma = 1.319$, $\delta = 4.623$, and $\alpha = -0.055$) were very close to the 3D-Heisenberg model and used to determine the field dependence of MCE.

II. EXPERIMENTAL DETAILS

$(Fe_{70}Ni_{30})_{89}B_{11}$ alloy nanoparticles were prepared by planetary ball milling (FRITSCH) at 600 rpm under Ar atmosphere from elemental Fe (99.99%, Sigma Aldrich), Ni (99.998%, Fisher ChemAlert Guide), and B (97%, Sigma Aldrich) powders. To prevent cold welding, a small quantity of ethanol was also added in the material mixture. The ball to powder ratio was 10:1. The vials and balls were made of zirconium oxide, and the volume of the vial was 125 ml, which contains 15 balls (10 mm in diameter). To prevent oxidation during heat treatment, the magnetic nanoparticles were sealed under high vacuum (10^{-5} Torr) in a quartz tube. The sealed tube was heated at 700 °C (γ- phase region)[21] for 2 h and quenched in water. The structure and phase were determined by X-ray diffraction (XRD) using a Bruker D8 Advance diffractometer (CuKα radiation). The composition was confirmed by energy dispersive X-ray spectroscopy using a JEOL JSM-7600F scanning electron microscope. To determine the particle size and morphology, transmission electron microscopy (TEM) was carried out on a JEOL 2010 TEM with an operating voltage of 200 kV. Samples were prepared by ultrasonically dispersing a small quantity of powder in hexane followed by placing a drop of the suspension on a holey carbon-coated copper grid, the sample is then dried in air. The magnetic properties were measured using a physical property measuring system (PPMS) (EverCool-II, Quantum Design), equipped with a vibrating sample magnetometer probe and an oven (model P527).

III. RESULTS AND DISCUSSION

A. Phase analysis

Fig. 1(a) shows the XRD patterns of $(Fe_{70}Ni_{30})_{89}B_{11}$ nanoparticles after 4, 5, 7, 8, and 10 h milling times. Rietveld refinement showed that the product after 4 h milling is a mixture of both body centered cubic (bcc) and fcc FeNiB phases. As milling time increased to 5 h, the intensity of the diffraction peaks increased slightly and shifted to higher "2θ" values (Fig. 1(b)), indicating greater crystallinity and lower cell volume. The mass fraction of the bcc phase reduced with milling time and only the γ-FeNi was observed after 10 h milling time (Fig. 1(b)).[22] The γ-phase has lattice parameters a = 3.59893(6) Å, V = 46.61465 Å^3, Z = 2, and space group Fm-3 m. In mechanical alloying, the composition ranges of the bcc and fcc phase regions were extended compared to their equilibrium range.[22] The average crystalline size, calculated by the Scherrer's formula, was ~18 nm and ~10 nm for bcc (4 h milling) and fcc (10 h milling) phases, respectively,[23] Fig. 1(c) shows the bright field transmission electron micrograph for $(Fe_{70}Ni_{30})_{89}B_{11}$ after 10 h milling time. The particle size is in the range of 6 to 17 nm with an

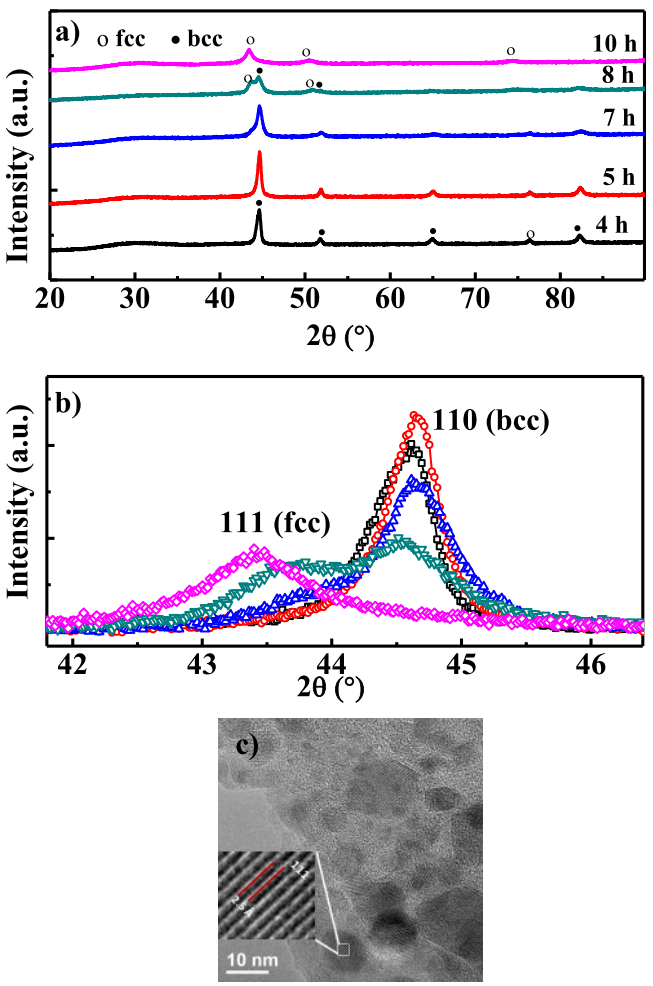

FIG. 1. (a) XRD patterns of $(Fe_{70}Ni_{30})_{89}B_{11}$ nanoparticles after milling times 4, 5, 7, 8, and 10 h under Ar atmosphere. (b) Higher magnification of 110(bcc) and 111(fcc) diffraction peaks. (c) Bright field TEM of γ-$(Fe_{70}Ni_{30})_{89}B_{11}$ nanoparticles with magnified inset showing lattice spacing corresponding to 111 planes.

average size of 12 nm, close to the value obtained from the XRD data. The lattice fringe of 2.5 Å, corresponding to the 111 planes of the fcc phase, is shown in the magnified portion of Fig. 1(c). The XRD and TEM results demonstrate that high speed ball milling has produced a nanocrystalline structure. Small particles are easy to suspend in fluids, even at high fields, thus providing versatile applications for heat transferring magnetic heat pumps and waste heat recovery.[24]

B. Magnetocaloric effect

Fig. 2(a) shows the temperature dependence of magnetization $M(T)$ of $(Fe_{70}Ni_{30})_{89}B_{11}$ nanoparticles with and without water quenching, under a field of 0.1 T. T_C of the as milled sample was above 400 K, whereas the quenched sample shows $T_C = 381$ K, as determined from the minima of the plot of dM/dT versus T (inset of Fig. 2(a)). Our T_C value for quenched nanoparticles is lower than that reported in the Fe-Ni phase diagram.[25] We attribute this change to atomic rearrangements, (short-range ordering or clustering by addition of boron) and quenching.[26] Recently, Moreno *et al.* also reported a large reduction in T_C of $Co_{62}Nb_6Zr_2B_{30}$ alloys by quenching.[27]

Fig. 2(b) shows the field dependence of magnetization $M(H)$ at $T = 10$ K. The sample exhibits soft ferromagnetic (FM) behavior with negligible hysteresis. The absence of field hysteresis in $M(H)$ is a great advantage for efficient magnetic cooling, since it permits high cycle operating frequency.[28] The inset of Fig. 2(b) shows the full cycle $M(H)$ isotherms from 100 to 600 K, which were used to determine ΔS_M using the Maxwell relation $\Delta S_M = \int_0^H (\partial M/\partial T)_H dH$. Fig. 3(a) shows the $-\Delta S_M$ versus T plots for field changes (ΔH) of 1, 2, 3, 4, and 5 T. At T_C equal to 381 K, $-\Delta S_M^{peak}$ increased from 0.51 to 2.1 J kg^{-1} K^{-1} for field changes $\Delta H = 1$ T and $\Delta H = 5$ T, respectively. These curves show a symmetric peak at T_C, indicating that the paramagnetic (PM) to FM phase transition is second-order.

RCP is calculated as the product of maximum entropy change and temperature at full width of half maximum, i.e., $RCP(S) = \Delta S_M \times \delta T_{FWHM}$. Because of the large δT_{FWHM} in our nanoparticles, the RCP increases from 89.8 to 640 J kg^{-1} for a field change ΔH equal to 1 T to 5 T, respectively. Fig. 3(b) shows the "$-\Delta S_M^{peak}$" (left) and RCP (right) as a function of ΔH. Recently, Ucar *et al.*[13] reported $-\Delta S_M$ and RCP values of 0.5 J kg^{-1} K^{-1} and 84 J kg^{-1} for a γ-$Fe_{72}Ni_{28}$ alloy for a field change ΔH of 1.5 T. The $-\Delta S_M$ and RCP values of our $(Fe_{70}Ni_{30})_{89}B_{11}$ nanoparticles for the same field change are 48% and 86% higher than $Fe_{72}Ni_{28}$. For $\Delta H = 5$ T, our RCP = 640 J kg^{-1} value is 36% higher than that of $Fe_{70}Ni_{30}$ and even larger than the benchmark magnetocaloric material, $Gd_5Ge_{1.9}Si_2Fe_{0.1}$ (630 J kg^{-1}).[28] Another benchmark material, Gd with 12 nm particle size has a RCP of 400 J kg^{-1}, which is ~46% less than our nanoparticle with the same average size.[14] In addition, we have made a comparison of the magnetocaloric properties of our nanoparticles with Gd, Pr_2Fe_{17}, Nd_2Fe_{17}, $(Fe_{70}Ni_{30})_{89}Zr_7B_4$ nanoparticles in Table I.

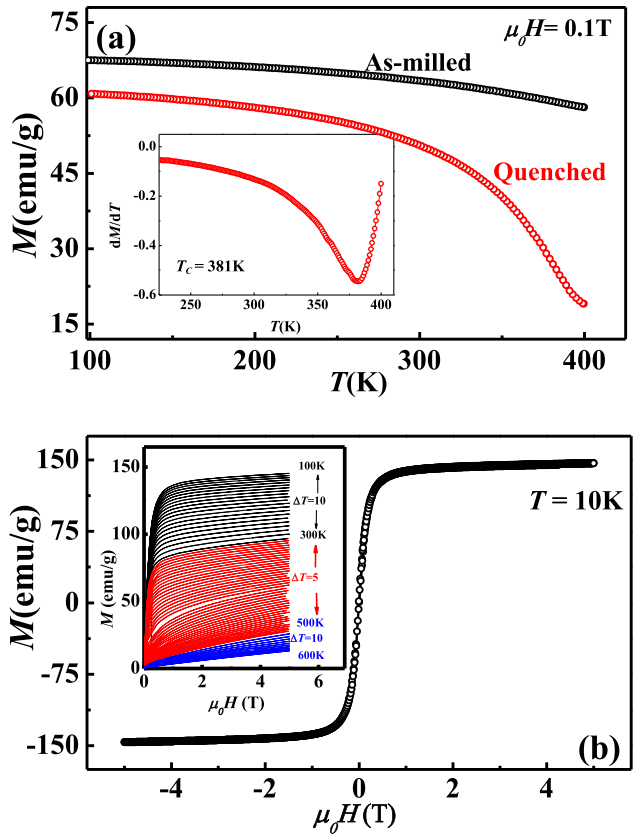

FIG. 2. (a) $M(T)$ versus T of as milled and water quenched of $(Fe_{70}Ni_{30})_{89}B_{11}$ nanoparticles for $\mu_0 H = 0.1$ T, the inset of (a) shows dM/dT versus T plot for the quenched sample. (b) M versus H at 10 K, the inset of (b) shows $M(H)$ isotherms from 100 to 600 K for the quenched sample.

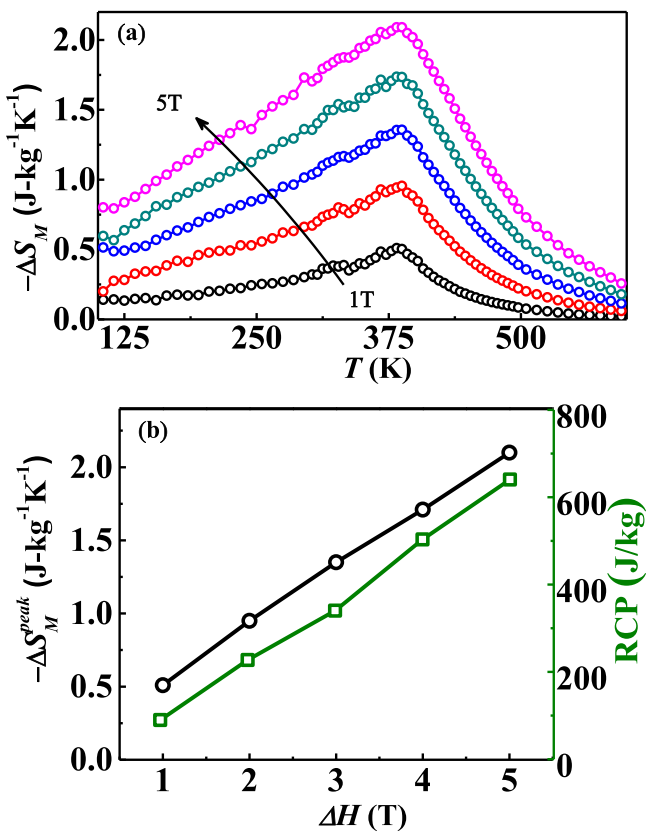

FIG. 3. (a) $-\Delta S_m$ versus T for quenched $(Fe_{70}Ni_{30})_{89}B_{11}$ nanoparticles for ΔH ranging from 1 T to 5 T. (b) ΔS_M^{peak} (left scale) and RCP (right scale) as a function of ΔH.

It can be concluded from Table I that our RCP value is higher than that of rare earth and FeNi based nanoparticles, with Curie temperature suitable for low grade waste heat recovery.

The enhanced spin disorder at surface is common in magnetic nanoparticles when particle size decreases in the same order of magnetic domain. On the other hand, surface atom experiences large anisotropy due to the broken symmetry of their surroundings, called Neel surface anisotropy.[32] The broadening in the ΔS_M versus T curve and therefore high RCP arises from the asymmetric nature of the exchange parameter and fluctuations in the interatomic spacing due to increased spin disorder at the surface of nanoparticles.[29,30] For small particle size, the total magnetization $M(H) = M_{core} + M_{surface}$ suggests that $\Delta S_M = \Delta S_{core} + \Delta S_{surface}$. Xi *et al.*, Garnin *et al.*, and Biasi *et al.* described in detail that how surface and core contribution are different in magnetic nanoparticles.[31–33] The ΔS_M of our nanoparticles (~12 nm size), which can be considered as a single domain, is the sum of the change in entropy of the core (ΔS_{core}) and the change in entropy of the disordered surface ($\Delta S_{surface}$). As the particle size decreases, the surface to volume ratio of the atoms increases. In nanoparticles, M_{core} decreases, while $M_{surface}$ is less dependent on T (less $\partial M_{surface}/\partial T$),[31] resulting in moderate ΔS_M and broad δT_{FWHM}. Mathew *et al.* also found an increment in broadening (δT_{FWHM}) in the ΔS_M versus T using nanostructuring of Gd and suggested that average nanocrystallite size can be used to tune the full width and half maximum of ΔS_M.[14]

Although second order transition materials (SOTM) generally exhibit lower ΔS_M^{peak} compared to first order transition materials (FOTM), their high RCP and absence of field hysteresis can make them better candidates for magnetic cooling.[34,35] The RCP is 4/3 times the cooling capacity $q = -\int_{T_1}^{T_2} \Delta S_M(T)_{\Delta H} dT$ of the material.[36] It indicates how much heat can be transferred from cold end (T_1) to the hot end (T_2) in one ideal thermodynamic cycle. Cooling power (CP), an important parameter for device applications is directly proportional to heat absorbed per cycle (q) and operating frequency. Engelbrecht *et al.* used different model materials in a device simulation and reported that a material with a broad peak in entropy change (large δT_{FWHM}) provides significantly better cooling power than a material with a sharp peak.[37] Cooling power for material with low ΔS_M and high δT_{FWHM} is about 50% more than that of material with high ΔS_M and low δT_{FWHM}, for the same normalized fluid flow rate. Thus, for a single regenerator, our material with broad temperature distribution of MCE is more attractive than with sharp ΔS_M peaks (low δT_{FWHM}). Franco *et al.* have reviewed the RCP and ΔS_M^{peak} for first and second order transition materials, our nanoparticles exhibit ΔS_M^{peak} comparable with most rare earth free SOTM and also exhibit higher RCP.[7] This implies that these nanoparticles could be potential candidates for magnetocaloric fluid based heat pumps and low grade waste heat recovery.

C. Critical behavior

1. Arrott plots

To understand the MCE, the nature of the magnetic phase transition responsible for the MCE needs to be determined. $M(H)$ isotherms for quenched nanoparticles were measured around T_C at each 2 K interval from 364 to 400 K (Fig. 4(a)). According to the Banerjee criteria, the order of the magnetic phase transition can be determined from the slope of the Arrott plot, M^2 versus H/M. A negative (positive) slope of the Arrott plot suggests that the magnetic phase transition is first (second) order.[38] Fig. 4(b) shows M^2 versus H/M curves for $(Fe_{70}Ni_{30})_{89}B_{11}$ nanoparticles. The nanoparticles exhibit a positive slope, indicating that the PM-FM phase transition is second order. However, all curves of the Arrott plots exhibit non parallel behavior, even at high magnetic fields. This indicates that the Arrott-Noakes equation[39] of state, i.e., $(H/M)^{1/\gamma} = (T - Tc)/Tc + (M/M_1)^{\beta}$, where M_1 is a materials constant, is not satisfied with critical exponents $\gamma = 1$ and $\beta = 0.5$. Generally, second order magnetic phase transition materials show straight parallel curves in the Arrott plot when spontaneous magnetization occurs due to long range ordering. In our case, however, the nonparallel nature of Arrott plots suggests the presence of inhomogeneous magnetic phases and short range order near T_C.

The critical behavior and nature of transition for our materials could be explained by the modified Arrott plot, as proposed by Noakes.[39] In the high magnetic field region, the effect of charge, lattice, and orbital degrees of freedom are suppressed in a ferromagnet and the order parameter can be

TABLE I. Curie temperature (T_C), grain size, change in entropy (ΔS_M) and relative cooling power (RCP) for promising magnetocaloric nanomaterials.

Nominal composition	T_C (K)	Grain size (nm)	μ_0H	$\lvert\Delta S_M\rvert$ J kg^{-1} K^{-1}	RCP (J kg^{-1})	Ref.
Gd	295	12	2	3.5	~180	14
Gd	295	12	5	7.2	~400	14
Pr_2Fe_{17}	290	11	1.5	~0.6	60	49
Pr_2Fe_{17}	~292	20	5	4.5	573	50
Nd_2Fe_{17}	340	11	1.5	~1	118	51
Nd_2Fe_{17}	340	14	1.5	1.6	87	51
$(Fe_{70}Ni_{30})_{89}Zr_7B_4$	353	20	1.5	0.7	…	19
$(Fe_{70}Ni_{30})_{89}Zr_7B_4$	353	20	5	~2.8	~330	19
$(Fe_{70}Ni_{30})_{89}B_{11}$	381	12	1	0.51	89.8	This work
$(Fe_{70}Ni_{30})_{89}B_{11}$	381	12	1.5	0.73	155	This work
$(Fe_{70}Ni_{30})_{89}B_{11}$	381	12	5	2.1	640	This work

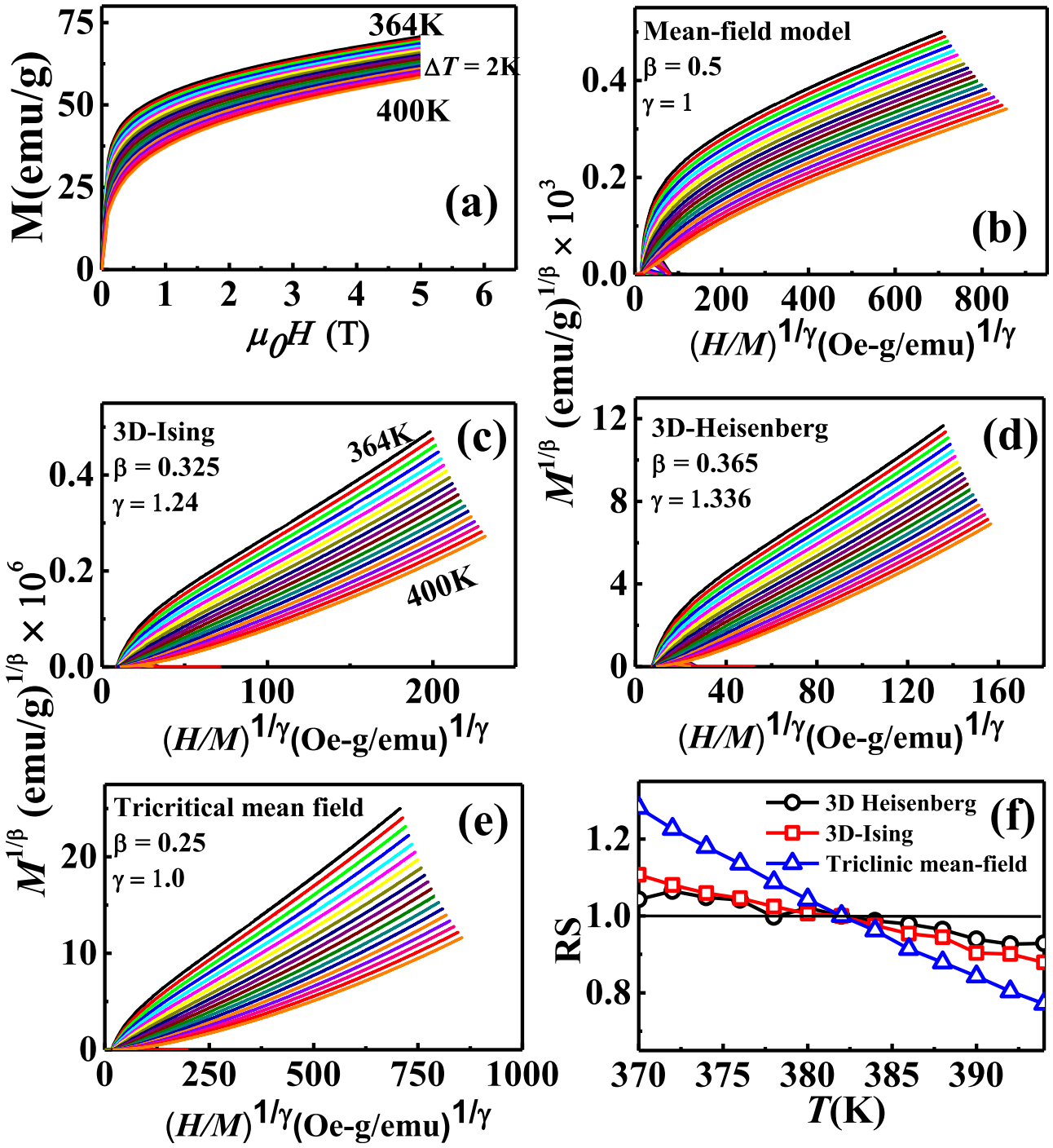

FIG. 4. (a) $M(H)$ isotherms around T_C, (b) Arrott plot (Mean-field model), (c) 3D-Ising model, (d) 3D-Heisenberg model, (e) triclinic mean field model, and (f) relative slope (RS) as a function of temperature.

identified with macroscopic magnetization.[40] Three models, i.e., 3D-Heisenberg model ($\beta = 0.365$, $\gamma = 1.336$), 3D Ising model ($\beta = 0.325$, $\gamma = 1.24$), and the tricritical mean field model ($\beta = 0.25$, $\gamma = 1.00$) were used to obtain experimental β and γ values (Figs. 4(c)–4(e)). To find the best model, the relative slopes (RS) of the straight lines, $RS = S(T)/S(T_C)$ were calculated. Fig. 4(f) shows the RS versus T plots for all three models. The value of RS for the tricritical and 3D-Ising models deviates from 1, while for the 3D-Heisenberg model it is much closer to 1. Therefore, the critical properties (β, and γ) and T_C of the $(Fe_{70}Ni_{30})_{89}B_{11}$ nanoparticles were calculated on the basis of the 3D-Heisenberg model.

2. Determination of critical exponents β, γ, δ, and α

Linear extrapolation from high fields to the intercept with the axis $(H/M)^{1/\gamma}$ for $T > T_C$ and $M^{1/\beta}$ for $T < T_C$, yields the spontaneous magnetization (M_S $(T,0)$) and the inverse magnetic susceptibility ($\chi^{-1}(T, 0)$). The critical exponents and T_C can be accurately determined from the Kouvel-Fisher (KF) method,[41] Eqs. (2) and (3).

$$\frac{Ms(T)}{dMs(T)/dT} = \frac{T - Tc}{\beta}, \tag{2}$$

$$\frac{\chi_0^{-1}(T)}{d\chi_0^{-1}(T)/dT} = \frac{T - Tc}{\gamma}. \tag{3}$$

According to this method, $M_s(dM_s/dT)^{-1}$ versus T and $\chi_0^{-1}(d\chi^{-1}/dT)^{-1}$ versus T should show straight lines with slope $1/\beta$ and $1/\gamma$, respectively. The value of T_C can be determined by extrapolation of these straight lines to the ordinate equal to zero on the T axis. Experimental data were fit with the Kouvel-Fisher method, yielding exponents $\beta = 0.364$ with $Tc = 380.96$ K and $\gamma = 1.319$ with $T_C = 381.32$ K (Fig. 5(a)). These values of critical exponents are in good agreement with the 3D-Heisenberg model.

The third critical exponent δ can be experimentally determined from the $M(H)$ at T_C (Fig. 5(b)). The slope $(1/\delta)$ of $\ln(M)$ versus $\ln(H)$ plot (the inset of Fig. 5(b)) yields $\delta = 4.60$. This exponent δ can also be determined by Widom's scaling relation[42] $\delta = 1 + (\gamma/\beta)$, which results in a δ value of 4.623. This value is close to our experiment value, implying that the critical exponents β and γ values are reliable.

The critical behavior near T_C was also verified by the universal scaling hypothesis. In the critical region, the magnetic equation of state[43] can be written as

$$m = f_{\pm}(h), \tag{4}$$

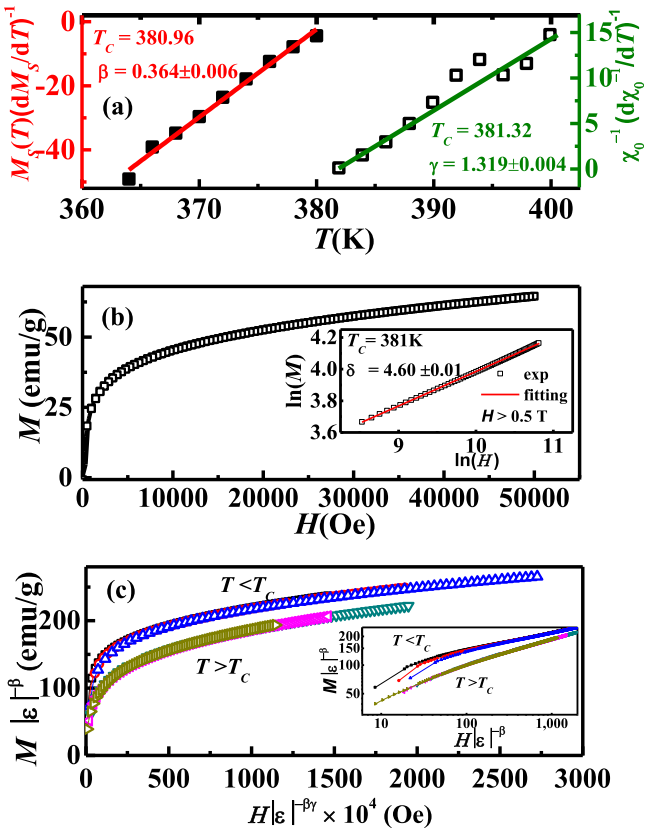

FIG. 5. (a) Kouvel-Fisher (KF) plot for $M_s.(dM_s/dT)^{-1}$ (left) and $\chi_0^{-1}.(d\chi_0^{-1}/dT)^{-1}$(right) versus T. (b) $M(H)$ at $T_C = 381$ K, inset shows ln$M$ versus ln$H$. (c) Scaling plots of $M(H)$ isotherms above and below T_C, using β and γ from the KF equations. Inset of (c) shows the same plot in log-log scale.

where m is the scaled magnetization, $m = |\varepsilon|^{-\beta}M(H, \varepsilon)$, h is the scaled field $h = |\varepsilon|^{-\beta\delta}H$ and ε is the reduced temperature $(T - Tc)/Tc$. Equation (4) implies that m as a function of h yields two universal curves: $f_+(h)$ for $T > T_C$ and $f(h)$ for $T < T_C$. The isothermal magnetization around T_C is plotted (Fig. 5(c)) as a prediction of the scaling theory. The experimental data fall on two curves, below and above T_C. The inset of Fig. 5(c) plotted on the log-log scale shows that all the points collapse into two universal curves. This indicates that our critical exponents and T_C are reliable and best match the 3D-Heisenberg model.

A fourth critical exponent (α), which is correlated to specific heat (C_H) and MCE (change in adiabatic temperature $\Delta T \propto 1/C_H$) can be defined by the homogeneous function approach: $\alpha = 2 - 2\beta - \gamma$, which yields $\alpha = -0.055$. For a negative value of α and a second order phase transition, short range disorder should not affect the sharpness of the transition, while long range disorder will smear the transition.[43] The experimental critical parameters for some materials and for theoretical models are listed in Table II. Most of the alloys reveal short range ferromagnetic disordered interaction with critical exponents near the 3D-Heisenberg model (Table II).

Nevertheless, some alloys such as $Fe_{77}Co_{5.5}Ni_{5.5}Zr_7B_4Cu$,[17] $Fe_{85}Ni_5Zr_{10}$,[44] and $Fe_{89.5}Zr_{10.5}$ (Ref. 45) exhibit the coexistence of short and long range interaction as the β value deviated from both of 3D-Heisenberg and mean field model.

D. Field dependence of ΔS_M (n) and RCP (N)

The mean field approach on the field dependence of the magnetic entropy change at T_C yields a prediction of $n = 2/3$.[18] In the case of our material, which does not follow the mean field model, the field dependence of ΔS_M and RCP has been obtained from the Arrott Noakes equation of state. Moreover, insight into the magnetocaloric properties with applied magnetic field can be delivered from acknowledged which of the theoretical models matches the experimental

TABLE II. Experimental values of the critical exponents of $(Fe_{70}Ni_{30})_{89}B_{11}$, results from theoretical models as well as critical exponents of other related ferromagnets. Abbreviations: KF: Kouvel-Fisher method, MAP: modified Arrott plots.

Material/model (method)	α	β	γ	δ	Ref.
$(Fe_{70}Ni_{30})_{89}B_{11}$ (KF)	−0.055	0.364	1.319	4.623	This work
3D-Heisenberg	−0.115	0.365	1.336	4.8	43
Mean-field theory	0.0	0.5	1.0	3.0	43
3D-Ising	0.11	0.325	1.241	4.82	43
Tricritical mean field	0.5	0.25	1	5	20
$Fe_{90}Zr_{10}$ (KF)	…	0.368	1.612	5.32	44
$Fe_{85}Ni_5Zr_{10}$ (KF)	…	0.425	1.323	4.11	44
$Fe_{77}Co_{5.5}Ni_{5.5}Zr_7B_4Cu$ (KF)	…	0.53	1.34	3.5	17
$Fe_{89.5}Zr_{10.5}$ (KF)	−0.93	0.47	2.0	5.31	45
$Fe_{88}Zr_8B_4$ (MAP)	…	0.39	1.38	…	52
Er_2Fe_{17} (MAP)	−0.59	0.42	1.74	5.1	53
Fe	−0.11	0.389	1.333	4.35	54
Ni	−0.10	0.378	1.34	4.58	55
Co	−0.095	0.435	1.225	3.35	56
Gd	0.04	0.381	1.196	3.615	43

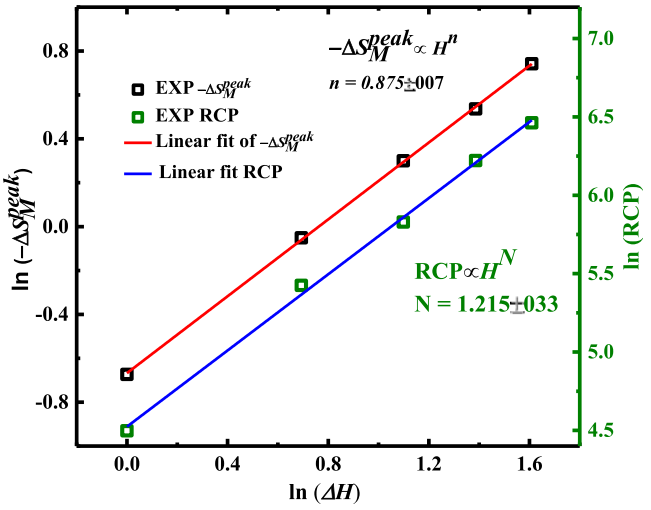

FIG. 6. Field dependence of change in entropy ΔS_M^{peak} (left scale) and relative cooling power, RCP (right scale) in ln-ln scale.

observations. The mean field model, 3D-Heisenberg model, 3D-Ising model, and tricritical mean field model yield n equal to 0.66, 0.68, 0.57, and 0.4, respectively. Fig. 6 shows the field dependence of the ΔS_M and RCP, which is measured by a linear fit of the values of ΔS_M and RCP for different fields on the ln-ln scale. The field dependence of RCP ($RCP \propto H^N$), i.e., the value of $N = 1.215$ calculated from the linear fit of experimental data agrees very well with the value obtained from the critical exponents using the 3D-Heisenberg model ($N = 1.216$). However, the value of n obtained from the slope of ΔS_M versus ΔH is 0.875, which is somewhat higher than that obtained from the critical exponents (0.62) and does not match any of the models. $La_{0.67}Ca_{0.33}Mn_{0.9}Cr_{0.1}O_3$ (Ref. 46) and $La_{0.6}Nd_{0.4}(CaSr)_{0.3}Mn_{0.9}V_{0.1}O_3$ (Ref. 47) also exhibit higher values of n from the slope of ΔS_M versus ΔH than those obtained from the modified Arrott plot. The magnitude values of ΔS_M and RCP depends not only on n and N but also on the proportionality factor (Eq. (1)). Large value of N (i.e., small δ) favors to get large RCP but in our material it is expected that proportionality factor between RCP and H, which depends on the other critical exponents dominates. These critical exponents depend on the dimensionality of the material, the number of components, and the range of microscopic interactions.[48]

IV. CONCLUSION

The magnetocaloric properties and critical behavior of FeNiB nanoparticles, with a Curie temperature suitable for low grade waste heat recovery was investigated. $(Fe_{70}Ni_{30})_{89}B_{11}$ nanoparticles possessing a fcc crystal structure and an average particle size of 12 nm were synthesized *via* ball milling. We find very high RCP, varying from 89.8 to 640 J kg^{-1} for a field change from $\Delta H = 1$ to 5 T in $(Fe_{70}Ni_{30})_{89}B_{11}$ nanoparticles. These values of RCP are larger than those of giant magnetocaloric materials. Absence of field hysteresis and broad $-\Delta S_M$ versus T behavior are added advantages of this material. We evaluated the critical exponents (α, β, γ, δ) through the modified Arrott plot and the Kouvel-Fisher plot. Our experimental results agreed well with the 3D-Heisenberg model. The field dependence of the RCP shows a $H^{1+1/\delta}$ dependence with the critical exponent δ value measured from 3D-Heisenberg model. Broad operating temperature range along with moderate change in entropy and very high RCP make these nanoparticles potential candidates for magnetic cooling applications. Moreover, these finding can be used as a point of reference for understanding the MCE and critical behavior of FeNiB nanoparticles.

ACKNOWLEDGMENTS

This research was conducted by NTU-HUJ-BGU Nanomaterials for Energy and Water Management Programme under the Campus for Research Excellence and Technological Enterprise (CREATE), that is supported by the National Research Foundation, Prime Minister's Office, Singapore.

[1]S. W. Lee, Y. Yang, H. W. Lee, H. Ghasemi, D. Kraemer, G. Chen, and Y. Cui, Nat. Commun. **5**, 3942 (2014).
[2]L. D. Zhao, S. H. Lo, M. G. Kanatzidis, Y. Zhang, H. Sun, G. Tan, C. Uher, C. Wolverton, and V. P. Dravid, Nature **508**, 373 (2014).
[3]S. Chu and A. Majumdar, Nature **488**, 294 (2012).
[4]X. Moya, S. K. Narayan, and N. D. Mathur, Nature Mater. **13**, 439 (2014).
[5]O. Gutfleisch, M. A. Willard, E. Brück, C. H. Chen, S. G. Sankar, and J. P. Liu, Adv. Mater. **23**, 821 (2011).
[6]J. Y. Law, V. Franco, and R. V. Ramanujan, Appl. Phys. Lett. **98**, 192503 (2011).
[7]V. Franco, J. S. Blazquez, B. Ingale, and A. Conde, Annu. Rev. Mater. Res. **42**, 305 (2012).
[8]J. Y. Law, V. Franco, and R. V. Ramanujan, J. Appl. Phys. **111**, 113919 (2012).
[9]V. K. Pecharsky and K. A. Gschneidner, Jr., Phys. Rev. Lett.**78**, 4494 (1997).
[10]L. H. Lewis and M. H. Yu, Appl. Phys. Lett. **83**, 515 (2003).
[11]Q. Zhang, B. Li, X. G. Zhao, and Z. D. Zhang, J. Appl. Phys. **105**, 53902 (2009).
[12]R. Caballero-Flores, V. Franco, A. Conde, K. E. Knipling, and M. A. Willard, Appl. Phys. Lett. **98**, 102505 (2011).
[13]H. Ucar, J. J. Ipus, V. Franco, M. E. McHenry, and D. E. Laughlin, JOM **64**, 782 (2012).
[14]S. P. Mathew and S. N. Kaul, Appl. Phys. Lett. **98**, 172505 (2011).
[15]R. E. Rosensweig, Int. J. Refrig. **29**, 1250 (2006).
[16]R. Kuldip, U.S. patent 5,462,685 (31 October 1995).
[17]V. Franco, R. Caballero-Flores, A. Conde, K. E. Knipling, and M. A. Willard, J. Appl. Phys. **109**, 07A905 (2011).
[18]V. Franco, J. S. Blázquez, and A. Condea, Appl. Phys. Lett. **89**, 222512 (2006).
[19]J. J. Ipus, H. Ucar, and McHenry, IEEE Trans. Magn. **47**, 2494 (2011).
[20]K. Huang, *Statistical Mechanics*, 2nd ed. (Wiley, New York, 1987).
[21]H. Ucar, J. J. Ipus, D. E. Laughlin, and M. E. McHenry, J. Appl. Phys. **113**, 17A918 (2013).
[22]C. Kuhrt and L. Schultz, J. Appl. Phys. **73**, 1975 (1993).
[23]P. Dutta, A. Manivannan, and M. S. Seehra, Phys. Rev. B **70**, 174428 (2004).
[24]R. E. Rosenweig, *Ferrohydrodynamics* (Cambridge University Press, 1985), p. 34.
[25]L. J. Swartzendruber, V. P. Itkin, and C. B. Alcock, J. Phase Equilib. **12**, 288 (1991).
[26]M. R. Gallas and J. A. H. Jornada, J. Phys.: Condens. Matter **155**, 162 (1991).
[27]L. M. Moreno, J. S. Blázquez, J. J. Ipus, J. M. Borrego, V. Franco, and A. Conde, J. Appl. Phys. **115**, 17A302 (2014).
[28]V. Provenzano, A. J. Shapiro, and R. D. Shull, Nature **429**, 853 (2004).
[29]N. J. Jones, H. Ucar, J. J. Ipus, M. E. McHenry, and D. E. Laughlin, J. Appl. Phys. **111**, 07A334 (2012).
[30]V. Chaudhary and R. V. Ramanujan, MRS Proc. **1708**(1) (2014).
[31]S. Xi, W. Lu, and Y. Sun, J. Appl. Phys. **111**, 063922 (2012).
[32]D. A. Garanin and H. Kachkachi, Phys. Rev. Lett. **90**, 065504 (2003).

[33]E. D. Biasi, C. A. Ramos, and R. D. Zysler, Phys. Rev. B **65**, 144416 (2002).
[34]C. M. Bonilla, J. H. Albillos, F. Bartolomé, L. M. García, M. Parra-Borderías, and V. Franco, Phys. Rev. B **81**, 224424 (2010).
[35]K. Pecharsky and J. Gschneidner, Appl. Phys. **90**, 4614 (2001).
[36]A. M. Tishin and Y. I. Spichkin, *The Magnetocaloric Effect and its Applications* (Institute of Physics Publishing, Bristol, 2003).
[37]K. Engelbrecht and C. R. H. Bahl, J. Appl. Phys. **108**, 123918 (2010).
[38]S. K. Banerjee, Phys. Lett. **12**, 16 (1964).
[39]A. Arrott and J. E. Noakes, Phys. Rev. Lett. **19**, 786 (1967).
[40]J. Fan, L. Ling, B. Hong, L. Zhang, and Y. Zhang, Phys. Rev. B **81**, 144426 (2010).
[41]J. S. Kouvel and M. E. Fisher, Phys. Rev. **136**, A1626 (1964).
[42]L. P. Kadanoff, Physics **2**, 263 (1966).
[43]S. N. Kaul, J. Magn. Magn. Mater. **53**, 5 (1985).
[44]T. D. Thanh, N. H. Dan, T. L. Phan, H. Kumarakuru, E. J. Olivier, J. H. Neethling, and S. C. Yu, J. Appl. Phys. **115**, 023903 (2014).
[45]W. Winchuh and M. Rosenberg, J. Appl. Phys. **61**, 4401 (1987).
[46]P. Nisha, S. S. Pillai, M. R. Varma, and K. G. Suresh, Solid State Sci. **14**, 40 (2012).
[47]A. Dhahri, F. I. H. Rhouma, S. Mnefgui, J. Dhahri, and E. K. Hlil, Ceram. Int. **40**, 459 (2014).
[48]R. K. Pathria and P. D. Beale, *Statistical Mechanics*, 3rd ed. (Elsevier Ltd., 2011).
[49]J. L. Sánchez-Llamazares, C. F. Sánchez-Valdés, G. J. Cuello, V. Franco, P. Gorria, and J. A. Blanco, J. Appl. Phys. **115**, 17A929 (2014).
[50]P. Gorria, J. L. Sánchez-Llamazares, P. Alvarez-Alonso, M. J. Perez, J. S. Marcos, and J. A. Blanco, J. Phys. D: Appl. Phys. **41**, 192003 (2008).
[51]P. Alvarez, P. Gorria, V. Franco, J. S. Marcos, M. J. Perez, J. L. Sánchez-Llamazares, I. P. Orench, and J. A. Blanco, J. Phys.: Condens. Matter **22**, 216005 (2010).
[52]P. Alvarez, J. S. Marcos, P. Gorria, L. F. Barquin, and J. A. Blanco, J. Alloys Compd. **504**, S150 (2010).
[53]P. Alvarez, P. Gorria, J. S. Marcos, M. J. Perez, J. L. Sánchez-Llamazares, and J. A. Blanco, J. Phys.: Condens. Matter **25**, 496010 (2013).
[54]S. Arajs, B. L. Tehan, E. E. Anderson, and A. A. Stelmach, Int. J. Magn. **1**, 41 (1970).
[55]G. Bohnke, S. N. Kaul, W. Kettler, and M. Rosenberg, Solid State Commun. **48**, 743 (1983).
[56]W. Rocker, R. Kohlhaas, and Z. Angew, Physics **23**, 146 (1967).